Ionics (2023) 29:497–504
https://doi.org/10.1007/s11581-022-04806-x

ORIGINAL PAPER

Electrochemical performance of SnO_2/C nanocomposites as anode materials for lithium-ion batteries

Yingqiang Fan[1] · Xiujuan Chen[2] · Laixi Zhang[2] · Jiakui Wu[1] · Linlin Wang[1] · Shurong Yu[2] · Mingliang Wu[2]

Received: 8 June 2022 / Revised: 15 October 2022 / Accepted: 23 October 2022 / Published online: 11 December 2022

Abstract

Carbon-coated SnO_2 nanocomposites were synthesized successfully by the hydrothermal method and carbonization at 500 °C with glucose and $SnCl_2{\cdot}2H_2O$ as precursor materials. The SnO_2/C nanocomposites were characterized by various techniques such as X-ray powder diffraction (XRD), scanning electron microscopy (SEM), high-resolution transmission electron microscopy (HR-TEM), Raman spectra, and electrochemical analyses. It was demonstrated that SnO_2/C-0, SnO_2/C-5, SnO_2/C-15, SnO_2/C-30, and SnO_2/C-50 had initial discharge capacities of 1359.2, 1626.8, 2124.9, 1525.8, and 1349.4 $mAhg^{-1}$, respectively. In particular, the SnO_2/C-15 sample exhibited excellent high reversible lithium storage capacity, good rate capability, and cycling stability. The electrodes show a long cycling ability and high charge/discharge capacity due to the presence of carbon.

Keywords SnO_2 · Carbon coating · Anode material · Lithium-ion battery · Hydrothermal synthesis

Introduction

As one of the most promising electrochemical energy conversion and memory devices, lithium-ion batteries (LIBs) have been widely used in electric vehicles, biomedical, military, and aerospace fields due to their high specific energy, low price, no memory effect, and long cycle life [1–5]. Unfortunately, commercial graphite is currently the main anode material for LIBs [6, 7], but it can hardly meet the growing market demand due to its defects such as low theoretical capacity (372 $mAhg^{-1}$) and easy formation of lithium dendrites [8–11]. Therefore, the development of electrode materials with higher energy density and good cycling stability has become one of the most attractive topics [12].

Among the many anode materials for LIBs, SnO_2 has been intensively studied owing to its abundant reserves, low price, simple synthesis, and high theoretical specific capacity (783 $mAhg^{-1}$) [13–17]. However, SnO_2 has some intrinsic disadvantages that limit their commercial application in LIBs, for example, the large volume expansion effect (300%) during charge/discharge leads to electrode pulverization and poor electronic conductivity during the lithiation/delithiation process [18–20].

In this context, much effort has been devoted to solve these problems [21–24]. The most common solution is to form composites with carbon materials [25, 26]. These carbon matrices not only increase the electrical conductivity of the negative electrode material but also effectively prevent the volume expansion of the electrode material, which greatly improves the cycling performance [27, 28]. Abouali [29] proved that ultrafine SnO_2 particles encapsulated in hollow nanochannels in an ordered mesoporous carbon (OMC) framework performed excellent cycling and multiplicity performance as anode materials for LIBs. Carbon nanofiber (CNF) and SnO_2 nanorod composites used as anode materials for lithium-ion batteries exhibited good electrochemical properties as reported by Abe [30]. Wang [16] found the coating of MnO_2 nanosheets on SnO_2@C hollow nanospheres to obtain SnO_2@C@MnO_2 hierarchical hollow hybrid nanospheres, which exhibited excellent electrochemical performance (644.5 $mAhg^{-1}$ after 200 cycles). The above researches show that the carbon-coated SnO_2 can improve the electrochemical properties of the material.

✉ Laixi Zhang
lx.zh@lut.edu.cn

[1] State Key Laboratory of Advanced Processing and Recycling of Non-Ferrous Metals, Lanzhou University of Technology, Lanzhou 730050, China

[2] School of Mechanical and Electronical Engineering, Lanzhou University of Technology, Lanzhou 730050, China

In this work, carbon-coated SnO_2 nanocomposites were synthesized by hydrothermal method. Here, we report the use of carbon-coated SnO_2 nanocomposites as anode for LIBs, which exhibit good electrochemical properties.

Experimental

Synthesis of SnO_2/C nanospheres

First, 4 mmoL $SnCl_2{\cdot}2H_2O$, 5 mmoL $Na_3C_6H_5O_3{\cdot}2H_2O$, and 2 mmoL NaOH were dispersed in the mixture of ethanol (20 mL) and water (20 mL). Then, 2 mmoL PVP and amount of glucose were added to the above suspension under magnetic stirring. Afterwards, the mixed solution was stirred at 25 °C for 30 min. The suspension was subsequently transferred to a 100 mL Teflon-lined stainless steel autoclave and kept at 180 °C for 12 h and then cooled to room temperature naturally. The as-synthesized samples were collected and washed with ethanol and deionized water several times. After that, the samples were dried at 70 °C for 10 h. Then, heat treated in argon flow at 500 °C for 3 h. Under the doping ratio of glucose and tin dioxide to 0wt%, 5wt%, 15wt%, 30wt%, and 50wt%, samples with different carbon coating contents have been prepared and recorded as SnO_2/C-0, SnO_2/C-5, SnO_2/C-15, SnO_2/C-30, and SnO_2/C-50, respectively.

Materials characterization

The crystallographic characteristics of the SnO_2/C were characterized by powder X-ray diffraction (XRD) from a Cu Kα radiation source; the 2-theta values were scanned in the range of 20–80° at a rate of 10° min^{-1} with a step size of 0.02°. Morphological features of the samples were observed by a JSM-2010 transmission electron microscope (TEM) operating at 200 kV accelerated voltage and a JSM-6700F cold field emission scanning electron microscope (SEM) at 5 kV. X-ray photoelectron spectroscopy (XPS) was performed on a spectrometer (Thermo Escalab 250Xi), and the binding energy scale was calibrated using a C 1 s peak at 284.8 eV.

Materials characterization

Electrochemical performance measurements were performed by assembling CR2023-type coin cells. The electrodes consist of 70 wt% active material, 20 wt% acetylene black, and 10 wt% polyvinylidene fluoride (PVDF). Lithium metal was served as the counter electrode. The electrolyte was 1 M $LiPF_6$ in 1:1:1 in volume ratio of ethylene carbonate (EC)/dimethyl carbonate (DMC)/ethyl methyl carbonate (EMC). The cells were assembled in an Ar-filled glovebox. Cyclic voltammetry (CV) was performed on an electrochemical workstation (CHI 660E) with a potential range of 0.01 ~ 3.00 V and a scan rate of 0.1 mVs^{-1}. Electrochemical impedance spectroscopy (EIS) measurements were conducted on a CHI 660E electrochemical workstation. The galvanostatic charge/discharge test was performed on the LAND CT2001A battery tester.

Results and discussions

Figure 1 displays the XRD patterns for the five samples. All diffraction peaks of SnO_2/C-0, SnO_2/C-5, SnO_2/C-15, SnO_2/C-30, and SnO_2/C-50 samples are matched well with the standard diffraction peaks of tetragonal rutile SnO_2 (JCPDS No. 41–1445) [31]. The diffraction peaks at 26.6°, 33.9°, 38.9°, 51.8°, 54.7°, 57.8°, 61.8°, 64.7°, 66.0°, 71.3°, and 78.7° were assigned to the (110), (101), (200), (211), (220), (002), (221), (112), (301), (202), and (321) crystal planes, respectively, and the sharp diffraction peaks indicate the strong crystallinity of SnO_2 nanoparticles. For carbon coating of SnO_2 nanospheres, no clear crystalline carbon phase can be detected in Fig. 1, indicating that the carbon layer is amorphous [32].

In order to examine the effect of the variation of carbon cladding content on the product morphology, five samples of SnO_2/C-0, SnO_2/C-5, SnO_2/C-15, SnO_2/C-30, and SnO_2/C-50 were observed using SEM, and the results are shown in Fig. 2. According to the figure, it can be found that the change of carbon coating content during the synthesis process has a significant effect on the morphology of the final spherical SnO_2/C. A slight agglomeration was

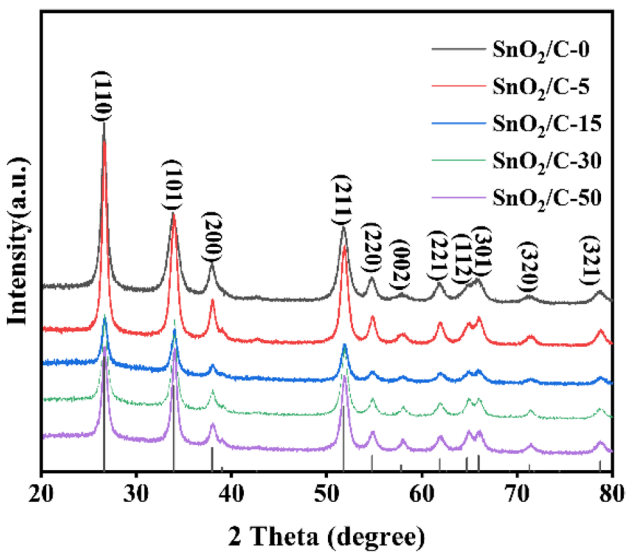

Fig. 1 XRD patterns of SnO_2/C-0, SnO_2/C-5, SnO_2/C-15, SnO_2/C-30, and SnO_2/C-50

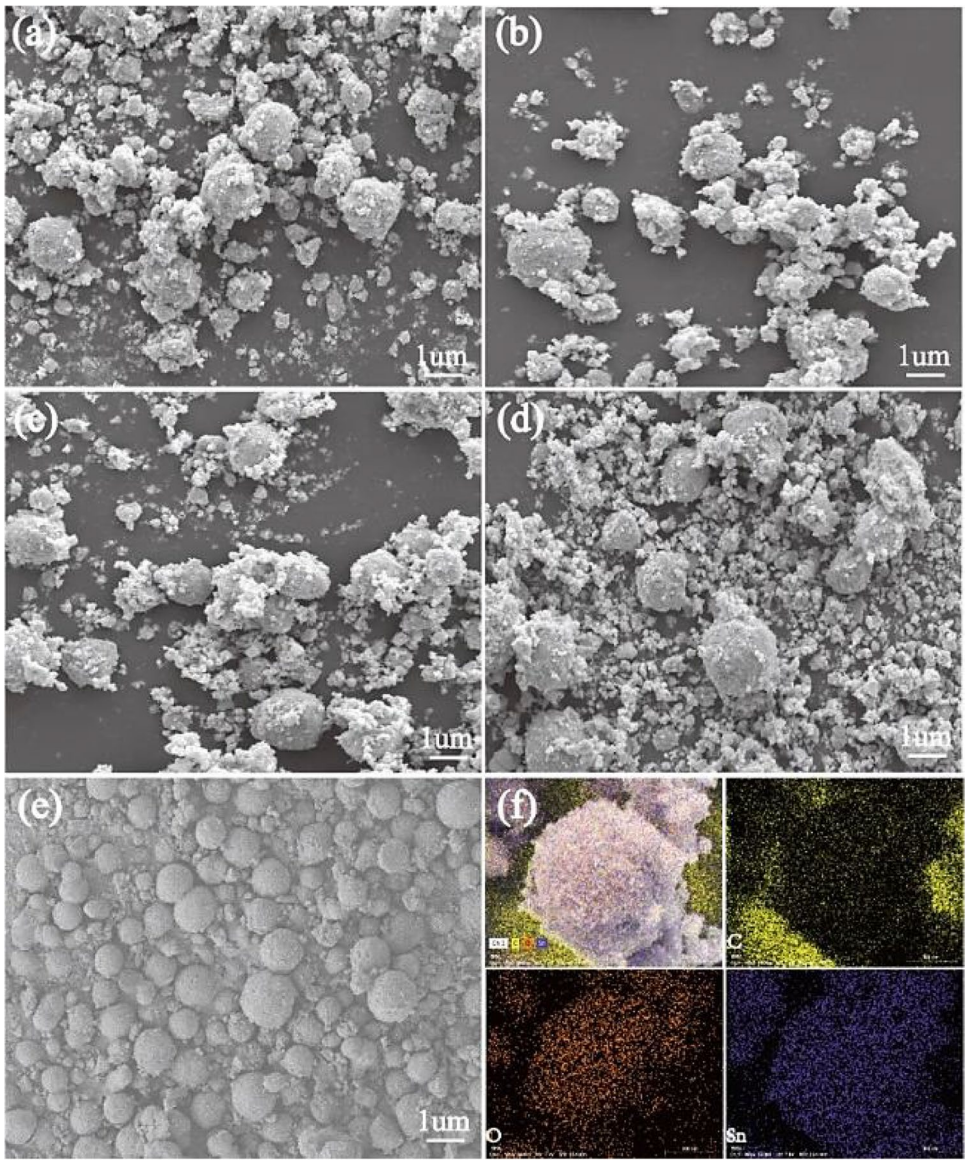

Fig. 2 SEM images of **a** SnO_2/C-5, **b** SnO_2/C-15, **c** SnO_2/C-30, **d** SnO_2/C-50, **e** SnO_2/C-0, and **f** EDS elemental mapping of SnO_2/C-15

found in the SnO_2/C-5 sample in Fig. 2a, and the particles were not uniform in size and poorly dispersed. As shown in Fig. 2b, the SEM image of the SnO_2/C-15 sample reveals that the product size is homogeneous and well dispersed, indicating that the morphology of SnO_2/C-15 was best. However, Fig. 2c, d shows SEM images of SnO_2/C-30 and SnO_2/C-50 with poor dispersion and inhomogeneous size of the products. Furthermore, it is observed that agglomeration of the material increases with the increase of the carbon cladding content. Thus, we can see that the SnO_2/C-15 sample has a better morphological structure than the electrode materials prepared with other carbon cladding contents. Figure 2f is the elemental image of SnO_2/C-15, showing that the spherical material is mainly composed of the three elements C, O, and Sn.

More close observation was performed by TEM. Figure 3 is the TEM images of the SnO_2/C-15 complex. Figure 3a shows the TEM bright-field image of SnO_2/C-15. It could be observed that the structure of the product is a large spherical structure of about 500 nm, which is aggregated from some small-size nanospheres with more complete spherical structure. Figure 3b shows a magnified image of the spherical edge, and it can be seen that the small-size nanospheres have a smooth surface with high integrity. The clear crystalline streaks in the small nanospheres with about 5–10 nm in diameter can be observed in Fig. 3c, which further demonstrates the well-crystallized structure of these SnO_2/C. The crystalline lattice spacing of 0.33 nm is identified corresponding to the (110) plane of SnO_2. The selected area electron diffraction (SEAD) pattern shows five different

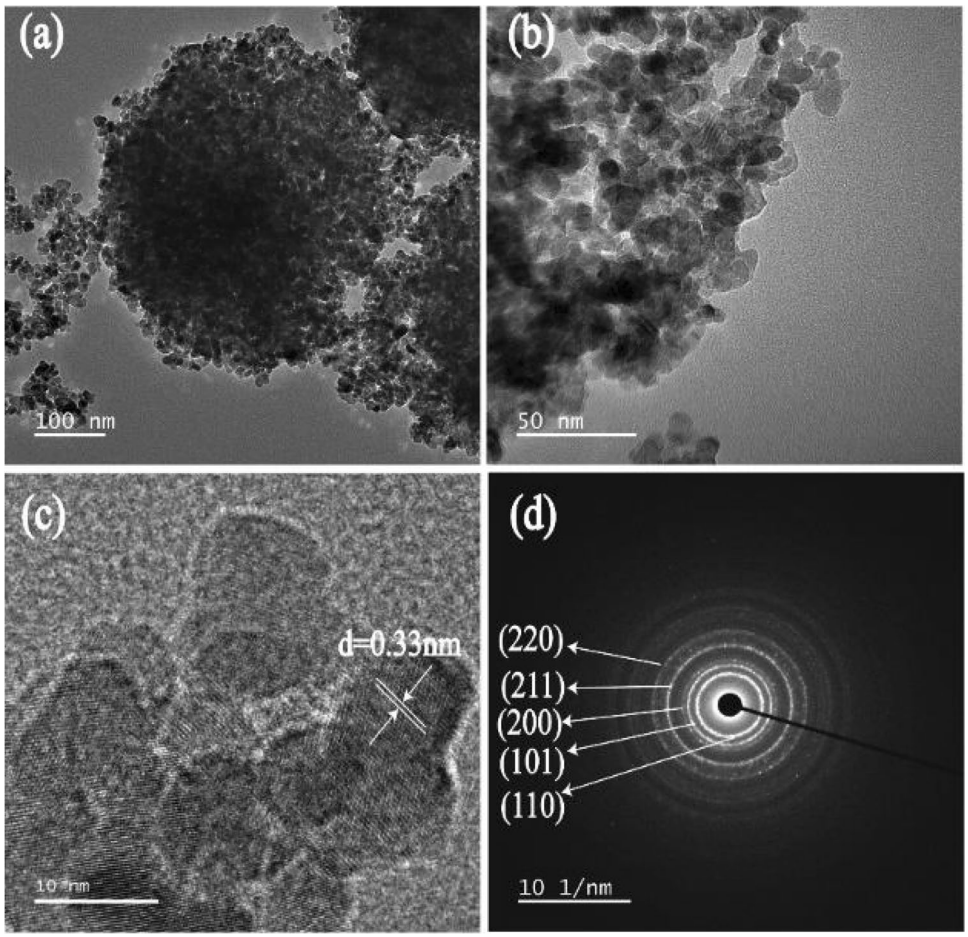

Fig. 3 TEM images of SnO_2/C-15 composite **a** and **b** TEM, **c** HRTEM, **d** SAED

diffraction rings, as shown in Fig. 3d, corresponding to the (110), (101), (200), (211), and (220) planes, and further confirms the correctness of the XRD analysis [33].

Figure 4 shows the Raman spectra of SnO_2/C-5, SnO_2/C-15, SnO_2/C-30, and SnO_2/C-50. The Raman peaks identified at 478 and 621 cm^{-1} were assigned to the Eg and A1g modes of anatase phase of SnO_2, respectively [34]. From the diagram, the peaks appearing near 1365 cm^{-1} and 1595 cm^{-1} correspond to the D-peak and G-peak of the samples, respectively. The ratio of the intensity of the D and G peaks (ID/IG) reflects the degree of disorder in the material; the higher values indicate a higher degree of disorder and the greater number of defects, and therefore, there are a greater number of active sites available for Li^+.

Figure 5a displays the XPS survey spectra of SnO_2/C-15. The peaks located at 284, 486, and 530 eV can be attributed to C1s, Sn 3d, and O1s spectra, respectively. Figure 5b shows a typical high-resolution XPS spectrum of Sn 3d. The two characteristic peaks appearing at 485.7 eV and 494.2 eV correspond to Sn $3d_{5/2}$ and Sn $3d_{3/2}$, respectively [22]. The high-resolution C1s spectrum in Fig. 5c is deconvoluted into three peaks at 284.55 eV, 283.65 eV, and 283 eV, indicating the presence of C = O, C-O, and C–C bonds, respectively.

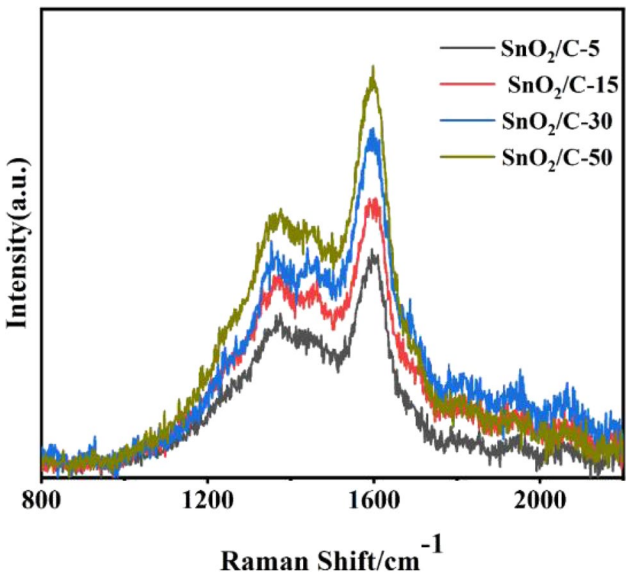

Fig. 4 Raman spectra of SnO_2/C-5, SnO_2/C-15, SnO_2/C-30, and SnO_2/C-50

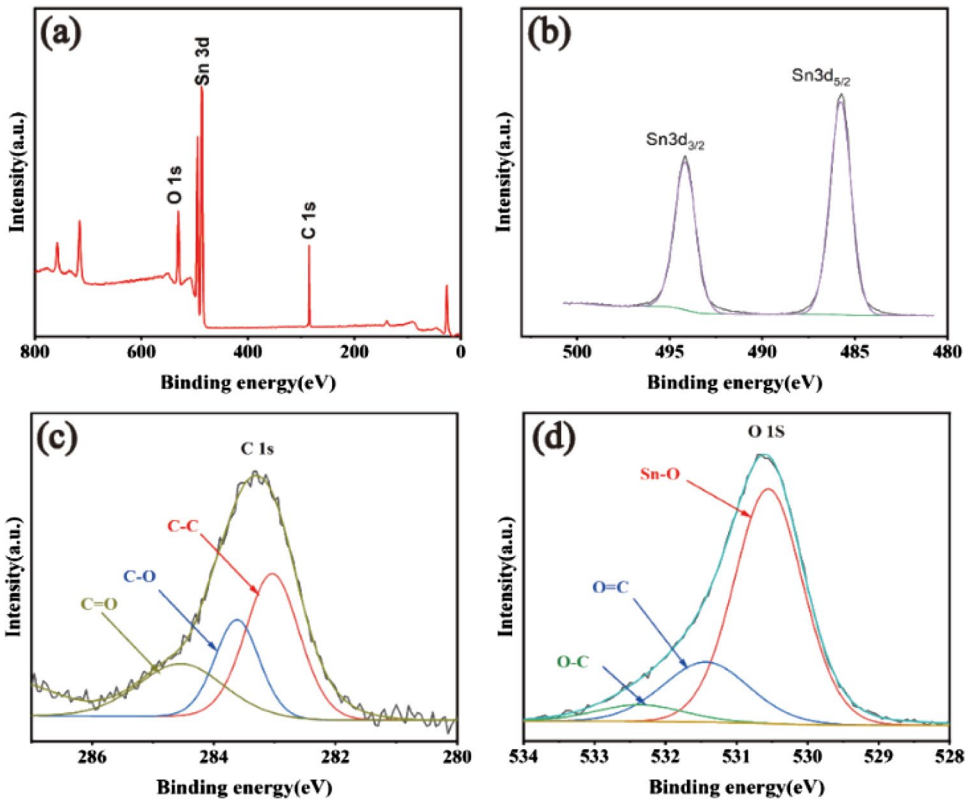

Fig. 5 **a** XPS spectra of SnO_2/C-15, and the corresponding high-resolution spectra of **b** Sn 3d, **c** C 1 s, and **d** O 1 s

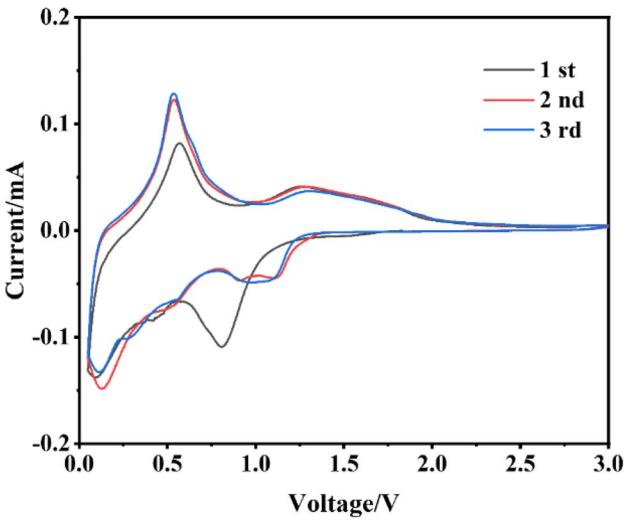

Fig. 6 CVs curves of SnO_2/C-15 at a scan rate of 0.1 mVs.$^{-1}$

In Fig. 5d, the high-resolution spectrum of O1s shows three chemical states: Sn–O (530.55 eV), O = C (531.5 eV), and O = C (532.5 eV) [35]. The XPS results indicate that the SnO_2/C-15 material consists of three elements, O, Sn, and C, and no other impurities are present, which corroborates with other characterizations.

Figure 6 displays the cyclic voltammograms (CVs) curves of the SnO_2/C-15 electrode in the voltage range of 0.01–3.0 V (for Li/Li$^+$) for the first three cycles at a scan rate of 0.1 mVs^{-1}. During the first cycle, a clear reduction peak can be seen at about 0.8 V. This is mainly due to the irreversible origination of the SEI film and partially reversible reaction between the lithium-ions and SnO_2($SnO_2 + 4Li^+ + 4e^- \rightarrow Sn + 2Li_2O$) [36]. The reduction peak near 0.1 V and the oxidation peak near 0.58 V correspond to the occurrence of reversible reactions between lithium ions and Sn ($xLi^+ + xe^- + Sn \leftrightarrow Li_xSn (0 \le x \le 4.4)$). The broad oxidation peak located near 1.28 V is attributed to the occurrence of a partially reversible oxidation reaction between Sn and Li_2O [37]. In the following two cycles, the curves overlapped with each other well, indicating an excellent cycle stability and reversibility of SnO_2/C-15.

Figure 7a compares the cycling performance of SnO2/C with different carbon cladding contents at the current density of 0.1C, and Fig. 7b compares the cycling performance of SnO_2/C-0 and SnO_2/C-15 at the current density of 1C. In Fig. 7a, the initial discharge capacity was found to be 1359.2, 1626.8, 2124.9, 1525.8, and 1349.4 mAhg^{-1} for SnO_2/C-0, SnO_2/C-5, SnO_2/C-15, SnO_2/C-30, and SnO_2/C-50, respectively. However the initial discharge capacity was found to be 1348.4 and 2025.7 for SnO_2/C-0 and SnO_2/C-15, as Fig. 7b. It can be seen that the SnO_2/C samples show higher capacity and better cycling stability than the original samples SnO_2/C-0, which indicates that the presence of carbon reduces the problem of crushing due to volume expansion

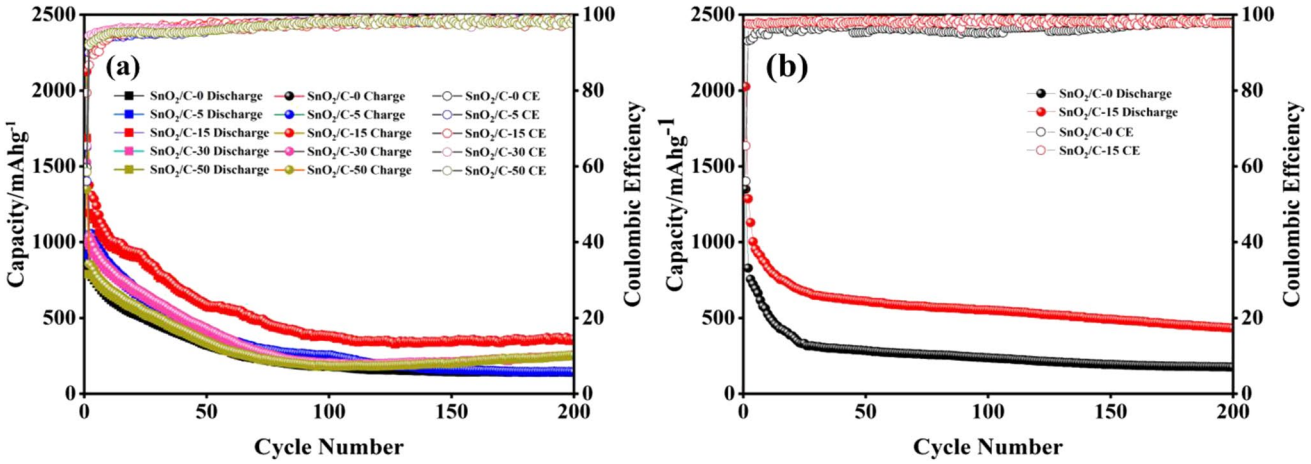

Fig. 7 **a** Cycling performances of SnO_2/C-0, SnO_2/C-5, SnO_2/C-15, SnO_2/C-30, and SnO_2/C-50 at the current density of 0.1C. **b** Cycling performances of SnO_2/C-0 and SnO_2/C-15 at the current density of 1C

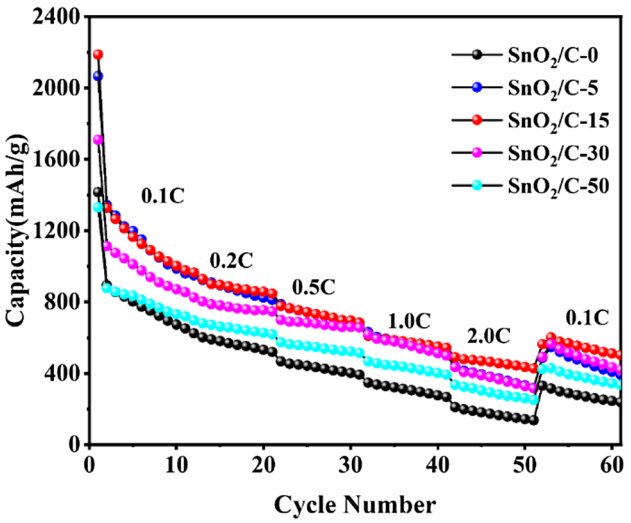

Fig. 8 Rate performances of SnO_2/C-0, SnO_2/C-5, SnO_2/C-15, SnO_2/C-30, and SnO_2/C-50 at different current densities ranging from 0.1C to 2C

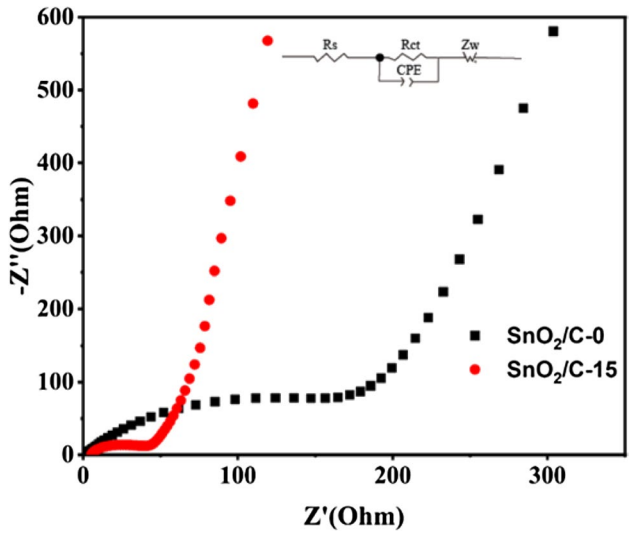

Fig. 9 Electrochemical impedance spectra (EIS) of the SnO_2/C-0 and SnO_2/C-15

during electrochemical processes [34]. Although the product capacity decayed rapidly within the first 20 cycles, the capacity of the samples gradually leveled off in the following cycles. After 200 cycles, SnO_2/C-15 showed a higher discharge capacity (361.4 $mAhg^{-1}$). These results suggest that the proper carbon-coated content is crucial to enhance the electrochemical performance, especially the SnO_2/C-15 exhibits good cycling stability.

The rate performance of the SnO_2/C electrode was investigated by discharging/charging at different current densities from 0.1C to 2C and back to 0.1C, as shown in Fig. 8. It is obvious that the capacity of SnO_2/C decreases gradually with the increase of the rate. For the sample of SnO_2/C-15, discharge capacity decreased from 1221.66 to 888.89, 728.81, 575.5, and 459.22 $mAhg^{-1}$ when the current density was increased from 0.1 to 0.2, 0.5, 1.0, and 2.0C, respectively, which is higher than the other samples. Then, the high discharge capacity of 547.32 $mAhg^{-1}$ can be regained as the current density was switched back to 0.1C, which indicates the high stability and excellent reversibility of the electrode.

The EIS profiles of the SnO_2/C-0 and SnO_2/C-15 are shown in Fig. 9. It can be seen from the figure that a semicircle in the high-frequency region and a linear in the low-frequency region were observed for all materials [38]. The semicircle in the high-frequency region can be attributed to the charge transfer resistance, while the straight line in the low-frequency region corresponds to the diffusion resistance of Li^+ in the electrode [39]. Comparing the electrochemical

impedance spectroscopy of SnO_2/C-0 and SnO_2/C-15, it was found that the charge transfer resistance and the diffusion resistance of SnO_2/C-15 were smaller than that of SnO_2/C-0. The results show that the carbon coating can effectively reduce the Li^+ transport distance and increase the transport rate, which can play a positive role in improving the electrochemical performance of SnO_2 electrode materials [40].

Conclusions

A series of SnO_2/C nanocomposite electrode materials have been successfully prepared. Owing to the introduction of carbon, the SnO_2/C nanospheres show excellent electrochemical properties. Notably, the nanospheres size of SnO_2/C-15 is only about 5–10 nm, and the first discharge specific capacity of it reached 2124.9 $mAhg^{-1}$ and still maintained discharge specific capacity of 361.4 $mAhg^{-1}$ after 200 cycles. The carbon layer presence leads to an effective improvement of electron conductivity and lithium ion transport capabilities. Meanwhile, the small size of nanospheres effectively reduces the lithium-ion transport distance, improves its transport rate, and reduces the volume expansion of SnO_2 during the cycling process. The method provides an effective preparation route for the practical application of SnO_2 in lithium-ion batteries.

Funding This work was supported by the Key Research Projects in Gansu Province (No. 17YF1GA020).

Declarations

Conflicts of interest The authors declare no competing interests.

References

1. Izumi A, Sanada M, Furuichi K et al (2012) Development of high capacity lithium-ion battery applying three-dimensionally patterned electrode [J]. Electrochim Acta 79:218–222
2. Huang Y, Zhu M, Huang Y et al (2016) Multifunctional energy storage and conversion devices [J]. Adv Mater 28(38):8344–8364
3. Liang J, Zhang L, XiLi D et al (2020) Rational design of hollow tubular SnO_2@TiO_2 nanocomposites as anode of sodium ion batteries [J]. Electrochim Acta 341:136030
4. Park J-S, Oh YJ, Kim JH et al (2020) Porous nanofibers comprised of hollow SnO_2 nanoplate building blocks for high-performance lithium ion battery anode [J]. Mater Charact 161:110099
5. Chao Z, Leiqiang Z, Ze Z et al (2021) Synthesis of the SnO2@ C@ GN hollow porous microspheres with superior cyclability for Li-ion batteries [J]. Chem Phys Lett 772:138566
6. Huang A, Ma Y, Peng J et al (2021) Tailoring the structure of silicon-based materials for lithium-ion batteries via electrospinning technology [J]. eScience 1:141–162
7. Huang C, Liu Y, Zheng R et al (2022) Interlayer gap widened TiS_2 for highly efficient sodium-ion storage [J]. J Mater Sci Technol 107:64–69
8. Shao L, Shu J, Lao M et al (2014) Hydroxylamine hydrochloride: a novel anode material for high capacity lithium-ion batteries [J]. J Power Sources 272:39–44
9. Ding R, Tian S, Zhang K et al (2021) Recent advances in cathode prelithiation additives and their use in lithium–ion batteries [J]. J Electroanal Chem 893:115325
10. Li X, Zhao R, Fu Y et al (2021) Nitrate additives for lithium batteries: mechanisms, applications, and prospects [J]. eScience 1:108–123
11. Xia H, Tang Y, Malyi OI et al (2021) Deep cycling for high-capacity Li-ion batteries [J]. Adv Mater 33(10):2004998
12. Dai Q, Gu C, Xu Y et al (2021) Self-sacrificing template method to controllable synthesize hollow SnO_2@ C nanoboxes for lithium-ion battery anode [J]. J Electroanal Chem 898:115653
13. Cho JS, Kang YC (2015) Nanofibers comprising yolk–shell Sn@void@SnO/SnO_2 and hollow SnO/SnO_2 and SnO_2 nanospheres via the Kirkendall diffusion effect and their electrochemical properties [J]. Small 11(36):4673–4681
14. Yang Z, Zhao S, Jiang W et al (2015) Carbon-supported SnO_2 nanowire arrays with enhanced lithium storage properties [J]. Electrochim Acta 158:321–326
15. Ma T, Yu X, Li H et al (2017) High volumetric capacity of hollow structured SnO_2@ Si nanospheres for lithium-ion batteries [J]. Nano Lett 17(6):3959–3964
16. Wang Y, Guo W, Yang Y et al (2018) Rational design of SnO_2@C@MnO_2 hierarchical hollow hybrid nanospheres for a Li-ion battery anode with enhanced performances [J]. Electrochim Acta 262:1–8
17. Wu C-P, Xie K-X, He J-P et al (2021) SnO_2 quantum dots modified N-doped carbon as high-performance anode for lithium ion batteries by enhanced pseudocapacitance [J]. Rare Met 40(1):48–56
18. Yu X, Yang S, Zhang B et al (2011) Controlled synthesis of SnO_2@ carbon core-shell nanochains as high-performance anodes for lithium-ion batteries [J]. J Mater Chem 21(33):12295–12302
19. Lee SH, Huang C, Grant PS (2021) Multi-layered composite electrodes of high power $Li_4Ti_5O_{12}$ and high capacity SnO_2 for smart lithium ion storage [J]. Energy Storage Materials 38:70–79
20. Zhu S, Huang A, Wang Q et al (2021) MOF derived double-carbon layers boosted the lithium/sodium storage performance of SnO_2 nanoparticles [J]. Nanotechnology 32(30):305403
21. Han C, Zhang B, Zhao K et al (2017) Oxalate-assisted formation of uniform carbon-confined SnO_2 nanotubes with enhanced lithium storage [J]. Chem Commun 53(69):9542–9545
22. Jiang B, He Y, Li B et al (2017) Polymer-templated formation of polydopamine-coated SnO_2 nanocrystals: anodes for cyclable lithium-ion batteries [J]. Angew Chem Int Ed 56(7):1869–1872
23. Pham-Cong D, Park JS, Kim JH et al (2017) Enhanced cycle stability of polypyrrole-derived nitrogen-doped carbon-coated tin oxide hollow nanofibers for lithium battery anodes [J]. Carbon 111:28–37
24. Zhang H, Li L, Li Z et al (2018) Controllable synthesis of SnO_2@ carbon hollow sphere based on bi-functional metallo-organic molecule for high-performance anode in Li-ion batteries [J]. Appl Surf Sci 442:65–70
25. Du X, Yang T, Lin J et al (2016) Microwave-assisted synthesis of SnO_2@ polypyrrole nanotubes and their pyrolyzed composite as anode for lithium-ion batteries [J]. ACS Appl Mater Interfaces 8(24):15598–15606
26. Huang Y, Pan Q, Wang H et al (2016) Preparation of a Sn@ SnO_2@C@MoS_2 composite as a high-performance anode material for lithium-ion batteries [J]. J Mater Chem A 4(19):7185–7189
27. Li X, Li X, Fan L et al (2017) Rational design of Sn/SnO_2/porous carbon nanocomposites as anode materials for sodium-ion batteries [J]. Appl Surf Sci 412:170–176

28. Zheng R, Yu H, Zhang X et al (2021) A $TiSe_2$-graphite dual ion battery: fast Na-ion insertion and excellent stability [J]. Angew Chem Int Ed 60(34):18430–18437
29. Abouali S, Garakani MA, Kim J-K (2018) Ultrafine SnO_2 nanoparticles encapsulated in ordered mesoporous carbon framework for Li-ion battery anodes [J]. Electrochim Acta 284:436–443
30. Abe J, Takahashi K, Kawase K et al (2018) Self-standing carbon nanofiber and SnO_2 nanorod composite as a high-capacity and high-rate-capability anode for lithium-ion batteries [J]. ACS Appl Nano Mater 1(6):2982–2989
31. Hong Y, Mao W, Hu Q et al (2019) Nitrogen-doped carbon coated SnO_2 nanoparticles embedded in a hierarchical porous carbon framework for high-performance lithium-ion battery anodes [J]. J Power Sources 428:44–52
32. Li Y, Zhao Y, Ma C et al (2016) Novel solvent-thermal preparation of a SnO_2 nanoparticles/expanded graphite multiscale composite with extremely enhanced electrical performances for Li-ion batteries [J]. Electrochim Acta 218:191–198
33. Li Y, Zhu S, Liu Q et al (2012) Carbon-coated SnO_2@ C with hierarchically porous structures and graphite layers inside for a high-performance lithium-ion battery [J]. J Mater Chem 22(6):2766–2773
34. Priyadharshini E, Suresh S, Gunasekaran S et al (2019) Investigation on electrochemical performance of SnO_2-Carbon nanocomposite as better anode material for lithium ion battery [J]. Physica B 569:8–13
35. Zhao X, Zhang J, Zhang J et al (2015) Construction of spongy antimony-doped tin oxide/graphene nanocomposites using commercially available products and its excellent electrochemical performance [J]. J Power Sources 294:223–231
36. Hu X, Wang G, Wang B et al (2019) Co_3Sn_2/SnO_2 heterostructures building double shell micro-cubes wrapped in three-dimensional graphene matrix as promising anode materials for lithium-ion and sodium-ion batteries [J]. Chem Eng J 355:986–998
37. Shiva K, Rajendra H, Subrahmanyam K et al (2012) Improved lithium cyclability and storage in mesoporous SnO_2 electronically wired with very low concentrations ($\leq 1\%$) of reduced graphene oxide [J]. Chem Eur J 18(15):4489–94
38. Han X, Li R, Qiu S et al (2019) Sonochemistry-enabled uniform coupling of SnO_2 nanocrystals with graphene sheets as anode materials for lithium-ion batteries [J]. RSC Adv 9(11):5942–5947
39. Tian F, Zhang Y, Liu L et al (2021) Thermally reshaped polyvinylpyrrolidone/SnO_2@ p-toluenesulfonic acid-doped polypyrrole nanocables with high capacity and excellent cycle performance as anode for lithium-ion batteries [J]. J Alloys Compd 867:159067
40. Tian Q, Chen Y, Zhang F et al (2020) Hierarchical carbon-riveted 2D@ 0D TiO_2 nanosheets@ SnO_2 nanoparticles composite for a improved lithium-ion battery anode [J]. Appl Surf Sci 511:145625